In-situ U-Pb isotope and REE analyses for zircons from ultrahigh temperature metamorphic rocks in the Kannak Complex, Kontum Massif, Vietnam.

Bui Thi Sinh, Vuong
Graduate School of Integrated Sciences for Global Society, Kyushu University

Osanai, Yasuhito
Division of Earth Sciences, Faculty of Social and Cultural Studies, Kyushu University

Nakano, Nobuhiko
Division of Earth Sciences, Faculty of Social and Cultural Studies, Kyushu University

Adachi, Tatsuro
Division of Earth Sciences, Faculty of Social and Cultural Studies, Kyushu University

他

https://doi.org/10.15017/2547988

出版情報：地球社会統合科学. 26 (2), pp.1-9, 2019-12-31. Graduate School of Integrated Sciences for Global Society, Kyushu University

『地球社会統合科学』第26巻 第2号（2019）1～9
Bulletin of the Graduate School of Integrated Sciences for Global Society, Kyushu University
Vol.26, No.2 (2019), pp. 1 ～ 9

In-situ U–Pb isotope and REE analyses for zircons from ultrahigh temperature metamorphic rocks in the Kannak Complex, Kontum Massif, Vietnam.

Vuong BUI THI SINH[1], Yasuhito OSANAI[2], Nobuhiko NAKANO[2], Tatsuro ADACHI[2], Ippei KITANO[2]

[1] Graduate School of Integrated Sciences for Global Society, Kyushu University, 744 Motooka, Nishi-ku, Fukuoka 819-0395, Japan

[2] Division of Earth Sciences, Faculty of Social and Cultural Studies, Kyushu University, 744 Motooka, Nishi-ku, Fukuoka 819-0395, Japan

Abstract

Zircons from two pelitic granulites (corundum–spinel-bearing garnet–cordierite–sillimanite and garnet–spinel–cordierite granulites) of the western Kannak Complex, Kontum Massif, Vietnam were analyzed for in-situ U–Pb isotope age dating and rare earth elements (REE) chemistry along with textural context by laser ablation inductively coupled plasma mass spectrometry. As the result, the correlation between zircon occurrence, its internal textural, U–Pb age and REE characteristics confirmed the ultrahigh temperature event during Permian–Triassic (230-260 Ma) and linked the age with the metamorphic process. The timing of peak metamorphism related with continental collision was constrained between *ca*. 250-260 Ma by the evidences of zircon inclusions in garnet from garnet–spinel–cordierite granulite and nearby cordierite–spinel symplectite from corundum–spinel-bearing garnet–cordierite–sillimanite granulite. The REE patterns of these zircons display the enrichment in the heavy REE (HREE) with gentle and steep positive slope, respectively. The youngest age group of *ca*. 230 Ma is yielded from the zircon contacting or included in secondary minerals such as chlorite or muscovite with the distinguishably depleted HREE, which corresponds to the timing of later intense hydration event during exhumation.

Keywords: In-situ zircon analyses, rare earth elements, U–Pb age, Kannak Complex, Kontum Massif

1. Introduction

The high temperature (HT) metamorphic rock with the amphibolite- to granulite-facies grade is one of the products by the continental collision during continental growth. It plays an important role in revealing the large-scale continental growth throughout a geological time. In particular, ultrahigh temperature (UHT) metamorphic rocks which underwent the extreme temperature condition beyond 900℃ provide the principal understanding of the development and stabilization of continents through the collisional process (Harley et al., 2016). However, the main task of metamorphic petrology does not terminate at discovering the process and condition of the metamorphism. Developing in the metamorphic petrology requires the connection of metamorphic condition to the chronometer with the precise and proper dating method to construct the framework of metamorphic evolution. In case of the UHT condition, in order to determine the timing of the peak metamorphism, the Zrn U–Pb isotope dating has been considered as a reliable method due to its high closure temperature (e.g., Harley et al., 2007, 2016). Zrn also can grow or (re) crystallize during the HT metamorphism via metamorphic solid-state reactions and/or partial melting or fluid (e.g., Harley et al., 2007). Therefore, the U–Pb Zrn ages can provide the timings of the metamorphic stages involved the Zrn growth or (re) crystallization. The major challenge in understanding the significance of the U–Pb ages is the connection with the occurrence of Zrn in the thin section and its texture. The occurrence of Zrn supplies the hint for the possible interaction between Zrn and surrounding minerals or some external mobile factor (fluid or melt). Besides, the texture of morphology and internal zoning pattern is a useful tool to identify the origin of Zrn such as igneous or metamorphic origin (e.g., Hoskin and Schaltegger, 2003). However, the U–Pb isotope dating is often applied to Zrn grains separated from the crushed samples since the abundant dates are easily and quickly obtained. The conventional method completely lacks in the relation of Zrn occurrence and its age, which prevents from interpreting the significance of Zrn U–Pb ages. Thus, the in-situ dating techniques from the thin section contributes to the direct combination of the occurrence, morphology, internal texture and U–Pb age of Zrn in order to precisely constrain the timing of the UHT metamorphic condition. As well as the intact textural relationship, trace element analyses (e.g., Y, REE) for Zrn give a help to decipher the growth environment. Therefore, in-situ Zrn chemical and chronological analyses provide a new sight to reveal the timeline of the UHT metamorphic process.

The Kontum Massif, which is a member of the Trans Vietnam Orogenic Belt (TVOB) (Osanai et al., 2008), has been known long time ago with a complicated metamorphic history which composed of various metamorphic rocks from greenschist- to granulite-facies (e.g., Osanai et al., 2004; Nakano et al., 2007, 2013). Of which, the Kannak Complex is concerned as the highest temperature metamorphic complex in the Kontum Massif, up to UHT granulite-facies that are characterized by a clockwise pressure–temperature (*P–T*) evolution. Previous studies have reported the dominant Permo–Triassic HT-UHT metamorphic event (*ca*. 230–260 Ma) in this complex in addition with the minor Ordovician–Silurian event one (*ca*. 430–460 Ma) only in the eastern part (e.g., Osanai et al., 2004; Nakano et al., 2007, 2013). Though the *P–T* evolution in the Kannak Complex is well established by petrological and mineral chemistry characteristics of these granulites, the *P–T*–time evolution has not been well established due to the lack of the relationship between the metamorphic ages and metamorphic stages. Understanding metamorphic evolution process of the Kannak Complex, will provide a significant contribution to reveal the tectonic evolution of the Kontum Massif in the TVOB as well as the growth of the Asian continent (Osanai et al., 2008). In this study, we investigate Zrn grains from two pelitic granulites in the western Kannak Complex to determine relative relation of Zrn growth and UHT metamorphic stage. Considering the relationship between modes of occurrence of Zrn grains along with their internal texture using cathodoluminescence (CL) image, U–Pb age and its trace element chemistry, it allows us to link the individual ages to the metamorphic evolution of the pelitic granulites in the western Kannak Complex. Minerals abbreviation in this study follows the works of Whitney and Evans (2010).

2. Geological setting and sample description

The Kannak Complex is exposed in the southeastern part of the Kontum Massif which is located in the southern part of the TVOB (Osanai et al., 2008), central Vietnam (Fig. 1a). The lithology of this complex mainly consists of the migmatitic pelitic gneiss/granulite (Fig. 2) with the minor mafic granulite (Osanai et al., 2004). Sometimes, the calc-silicate rock is also recognized in the intercalation within the pelitic rocks (Osanai et al., 2004). The metamorphic grade decreases from the western to eastern part. The HT to UHT granulite-facies metamorphic rocks found in the western part around An Khe town (Fig. 1b) and lower grade of amphibolite- to granulite-facies metamorphic rocks in the eastern part in Ba To to Qui Nhon (Fig. 1b) (Osanai et al., 2004; Nakano et al., 2007). The highest metamorphic condition was obtained from Grt–Opx–Sil granulite in the western at 1050 ℃ and 12 kbar (Osanai et al., 2004). In the eastern Kannak Complex, the temperature condition increases from the north (*ca*. 800 ℃) to

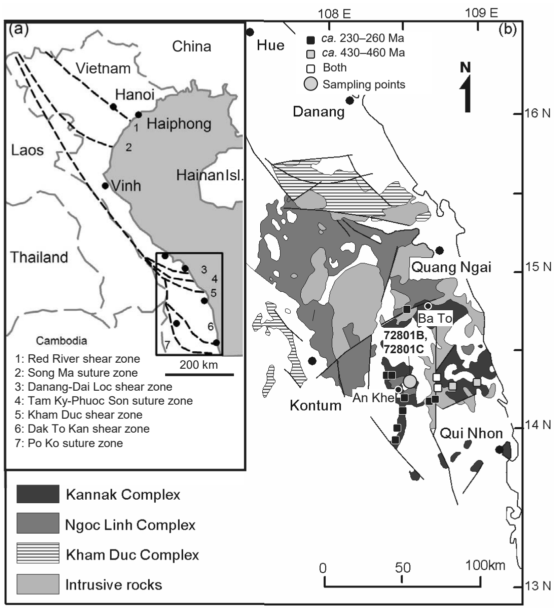

Figure 1

the south (*ca*. 900 ℃) with the lower pressure condition (at 6.3–8.4 kbar) (Nakano et al., 2007). The pelitic granulite usually accompanies with Grt-bearing S-type tonalite so-called Plei Man Ko granite (Owada et al., 2006, 2016).

In this study, we analyzed Crn-Spl-bearing Grt-Crd-Sil granulite (72801B) and Grt-Spl-Crd granulite (72801C) collected from the western Kannak Complex (Fig. 1). These samples are associated with migmatitic texture or leucocratic pod (Fig. 2). The metamorphic condition was estimated for the similar rock type in this location, at 915–970 ℃ and 11 kbar (Nakano et al., 2007). The Crn-Spl bearing Grt-Crd-Sil granulite (72801B) contains Grt, Crd, Sil,

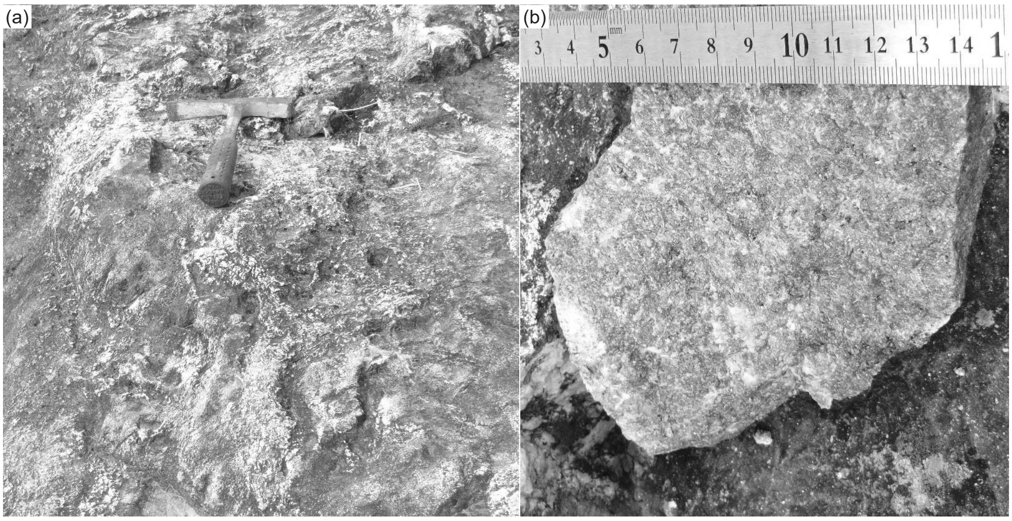

Figure 2

Spl, Pl, Kfs and minor Qz, Crn, Zrn, Ap, Ilm and Mag (Figs. 3a-d). Grt porphyroblast is mostly replaced by Crd, Crd-Spl symplectite or secondary Chl and Bt (Fig. 3a). Sil presents as both fibrolite in Grt and nematoblastic crystal in the matrix (Figs. 3a and 3d). Mostly, Crd is altered into Ms or pinite (Fig. 3e) with the minor remained primary Crd in contacting with Grt and Sil (Figs. 3a-b). Spl occurs only as symplectite surrounding Grt or between Grt and Sil (Figs. 3a, 3b and 3d). Sometime, the subhedral to euhedral Crn is recognized in contacting with Bt and/or Mag (Fig. 3b). Anhedral secondary And is also present in the matrix and replaced by Ms (Fig. 3c). Equant Zrn is abundantly included in Sil, Bt, Pl, Qz or in the matrix contacting with Ms, Chl, pinite or Crd-Spl symplectite (Figs. 3a, 3d-e). The Grt-Spl-Crd granulite (72801C) also shares quite similar petrographical features to those of Crn-Spl-bearing Grt-Crd-Sil granulite except the absence of Crn and occurrence of Sil and Spl (Figs. 3f-h). In this sample, Sil occurs only as inclusions in Grt; anhedral dark green Spl mainly intercalates with Grt (or as minor inclusion in Grt) or in contact with Pl and Mag (Fig. 3f). Subhedral Pl is also obviously observed in this sample (Fig. 3f). Isometric, euhedral ("soccer ball" shape) Zrn grains, present as inclusions in Pl, Grt or along the Grt crack, or in contact with Chl, Kfs, Pl or pinite (Figs. 3g-h).

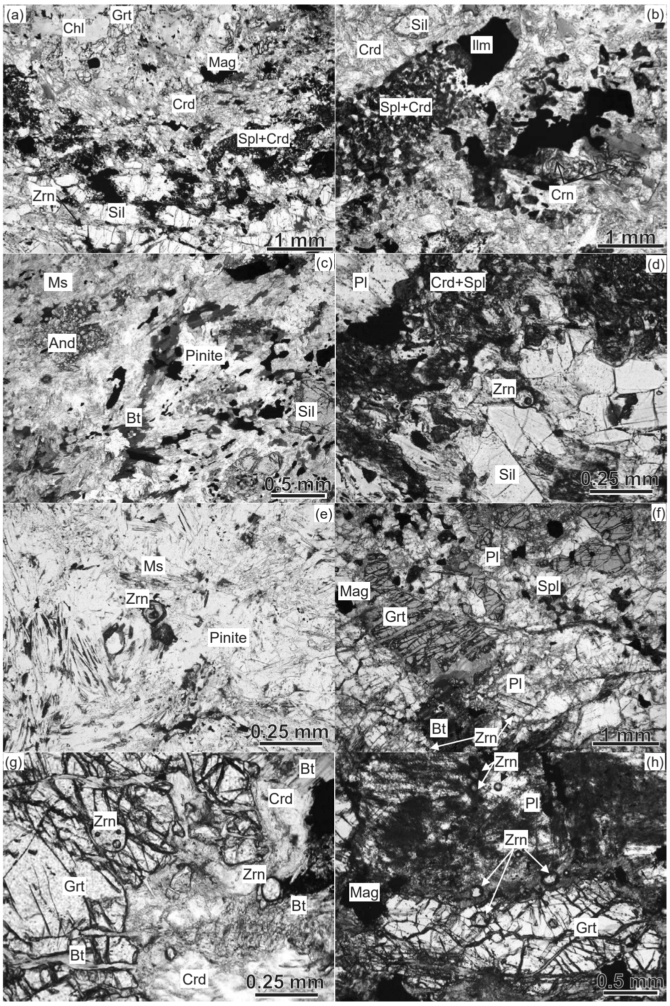

Figure 3

3. U–Pb Zrn dating and REE characteristics

U–Pb dating and REE analyses were conducted on Zrn grains from the polished thin section using an Agilent 7500cx quadrupole inductively coupled plasma mass spectrometry (ICP-MS) at Kyushu University, Japan. For the U–Pb dating, the laser ablation system of a pulsed 193 nm ArF Excimer laser was applied with a repetition rate of 8 Hz, output of 30 % and the spot size of 20 and 25 μm in diameter. The calibration and reference standards of 91500 (Wiedenbeck et al., 1995) and FC-1 (Paces and Miller, 1993) were used, respectively. Besides, the New Wave Research UP-213 Nd-YAG UV (213 nm) was performed for REE analyses. The analytical procedures for REE analyses are followed Nakano et al. (2010). Each Zrn grain was analyzed REE concentration by the spot size of 30 to 40 μm. The locations of Zrn were determined in polished thin section through the microscopic observation or back scattered electron (BSE) observations using an energy-dispersive spectroscopy-equipped scanning electron microprobe (JEOL JSM-6390-JED2300). The internal texture of Zrn was displayed by CL imaging through a CL detector (Gatan MiniCL). Age calculation was conducted using the software Isoplot/Ex (Ludwig, 2008). The error for each single spot is reported at 2 sigma intervals while the pooled ages are given at 95 % confidence levels. In this study, the concordant data is determined as one with less than 5 % discordance and plotted within 2 sigma of the concordia curve. The representative CL images of analyzed Zrn with obtained U–Pb age and Th/U ratio and concordia diagram are shown in Fig. 4 and Fig. 5, respectively.

The modes of occurrence and internal texture of analyzed Zrn grains were carefully investigated. Zrn grains from two samples of Crn–Spl-bearing Grt–Crd–Sil granulite (72801B) and Grt–Spl–Crd granulite (72801C) share the similarity in the external and internal texture characteristics. Abundantly, these Zrn are included in Bt, Pl, Qz or in contacting with Ms, Chl, pinite for both samples, with minor occurrence as inclusions in Sil or beside Crd–Spl symplectite in Crn–Spl-bearing Grt–Crd–Sil granulite (72801B), and as inclusions in Grt (along the crack) in Grt–Spl–Crd granulite (72801C). For the external features, they are isometric, equant to ovoid Zrn, colorless to yellowish, 50–200 μm across. In term of internal texture, the CL investigation revealed five domains. (1) The first small domain is observed as bright core (c) with irregular shape which is not always visible in all Zrn grains (Fig. 4a). The core displays the chaotic zoning pattern which is truncated by the first overgrowth domain (ov1). (2) The first overgrowth (ov1) on the cores (c) has a medium to low CL emission and displays chaotic zoning or unzoned internal texture (Figs. 4a-b, 4g). The boundary between the core and ov1 is often marked by an irregular light band. (3) The volumetrically most dominant zone is the second overgrowth (ov2) which is characterized by polygonal shape, high CL emission and concentric sector zoning (Figs. 4b-g). The boundary between the first (ov1) and second (ov2) overgrowth is sharp (Figs. 4b and 4g). (4) A few grains in contacting with Chl or Ms have a third, mainly idiomorphic overgrowth (ov3), which has a very low CL emission (Figs. 4b and 4f). (5) Some Zrn exhibits patchy zone (pz), in association with secondary mineral such as Chl, Bt, Ms or pinite (Fig. 4a). Except the small dark core and ov1, all domains of ov2, ov3 and pz were analyzed. Firstly, in Crn–Spl-bearing Grt–Crd–Sil granulite (72801B), seven analyses from ov2 of Zrn inclusions in Bt and Qz give the $^{206}Pb/^{238}U$ concordant data varying between *ca.*

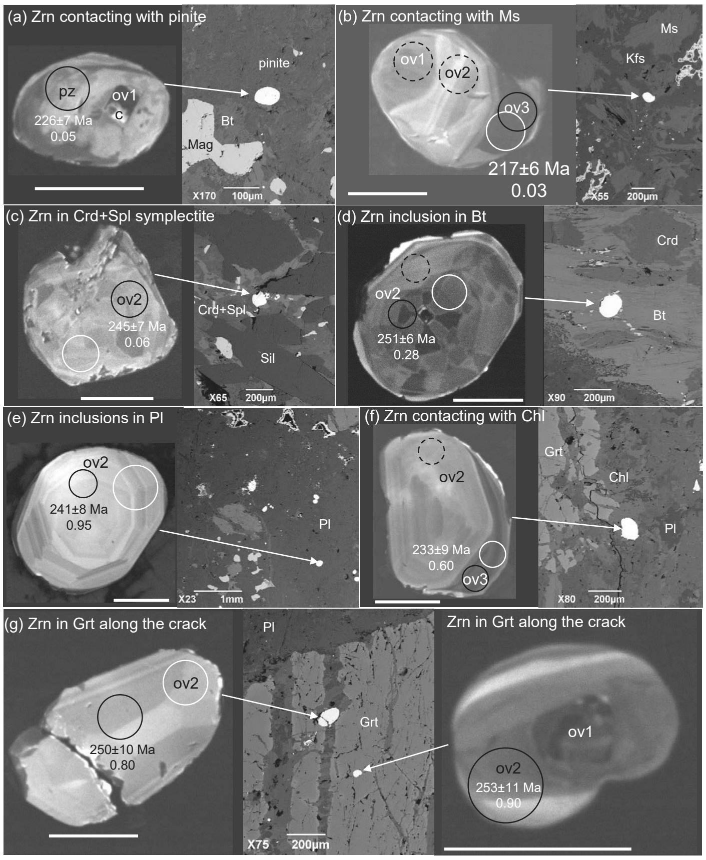

Figure 4

240–260 Ma, yield a concordia age of 251.7 ± 4.2 Ma (MSWD = 0.015) with scattered Th/U ratios of 0.06–0.64 (Fig. 5a). Seven data obtained from ov2 of Zrn in pinite pool at the similar concordia age of 251.3 ± 4.3 Ma (MSWD = 0.20) and Th/U ratios of 0.08–0.64 (Fig. 5a). Three measurement from ov2 of Zrn in Spl–Crd symplectite provide the clustered age at *ca*. 250 Ma with Th/U ratios of 0.06–0.18 (Fig. 5a). Six analyses from pz and ov3 of Zrn in contacting with Ms or Chl show the broad peak at *ca*. 230 Ma with scattered Th/U ratios of 0.05–0.36 (Fig. 5a). For the Grt–Spl–Crd granulite (72801C), fifteen dates collected from ov2 domain for Zrn inclusions in Pl represent the concordia age of 253.0 ± 2.4 Ma (MSWD = 0.50) and Th/U ratios of 0.02–1.29 (Fig. 5b). Eleven data obtained from ov2 of Zrn in Grt along the crack pool at the concordia age of 256.3 ± 3.0 Ma (MSWD = 0.11) and Th/U ratios of 0.03–1.13 (Fig. 5b). Finally, eleven measurements from ov2 and ov3 of Zrn in contacting with Chl give the similar isotopic ages which provide the concordia age of 229.3 ± 2.4 Ma (MSWD = 0.11) with Th/U ratios of 0.19–1.17 (Fig. 5b).

The REE characteristics are also investigated for some representative Zrn grains in the different occurrences. The result is present in the REE pattern diagram which is normalized to chondrite values (McDonough and Sun, 1995) in Figure 6. For the Crn–Spl-bearing Grt–Crd–Sil granulite (72801B), all Zrn grains display the fractionated REE patterns typified by the enrichment in HREE compared with middle (MREE) and light REE (LREE) with negative Eu anomalies and negligibly positive Ce anomalies (Fig. 6a). However, REE pattern is slightly different from each Zrn domain and occurrences. Of which, the ov2 Zrn inclusion in Bt or Qz is characterized by the slightly steep pattern (Lu_N/Gd_N = 2.8–4.3 at Gd_N of 57–109) with a modest enrichment in LREE (Ce_N of 3–4) and HREE. Besides, the REE pattern from ov2 Zrn occurring in the Crd–Spl symplectite shows the strong positive slope (Lu_N/Gd_N = 7.4–21.4 at Gd_N of 42–86) with the depleted LREE (Ce_N of around 1) and highly elevated HREE. In contrast, the REE pattern obtaining from ov3 and pz domains of Zrn contacting with Chl and Ms preserves a slight depleted to flat HREE pattern with Lu_N/Gd_N = 0.5–1.7 at Gd_N of 70–99 and inconsiderably high LREE (Ce_N of 1.8–3.5). In regard to the Grt–Spl–Crd granulite (72801C), analyses from ov2 domains of Zrn inclusions in both Pl and Grt (along the crack) display the similar REE pattern (Fig. 6b). It is characterized by considerably steep REE pattern with the depletion in LREE and enrichment in HREE (Lu_N/Gd_N = 3.1–5.2 at Gd_N of 38.2–70.4). The strong positive Ce anomalies and negative Eu anomalies are also recognized in these patterns. On the contrary, the analyzed ov3 domain of Zrn within/contacting with Chl preserves a depleted HREE pattern with Lu_N/Gd_N = 0.5–51.5 at GdN of 59–86 (Fig. 6b).

4. Discussion and concluding remarks

The in-situ analyses of Zrn from two pelitic granulites (72801B and 72801C) in the western Kannak Complex confirm the distinguishable REE and U–Pb ages features in the relationship with mode of occurrences and internal textures, which allows us to discuss growth/ (re) crystallization phases of Zrn during the UHT metamorphism. All analyzed Zrn grains from these two pelitic granulites (72801B and 72801C) exhibit the isometric, euhedral ("soccer ball") or equant shape in the external morphology (Figs. 3c-e, 3g-h and 4), which is typical for Zrn in the HT, granulite-facies metamorphic rocks (Hoskin and Schaltegger, 2003; Harley et al., 2007; Rubatto, 2017). Secondly, the CL images reveal a sequence internal textures: an initial low luminescence growth zone (ov1) (sometimes overgrowing an inherited core), sequentially overgrown by a bright sector zoned domain (ov2) and finally followed by dark unzoned one (ov3) or patchy zoned domain (pz) (Fig. 4). Of which, the second overgrowth of Zrn (ov2) with the polygonal zoning (Figs. 4b-g) is considered to be formed at the HT condition and with the presence of melt (e.g., Hermann and Rubatto, 2003; Harley et al., 2007). Therefore, the obtained age groups of *ca.* 230–260 Ma (Fig. 5) from these Zrn are considered as metamorphic ages. In both samples, the youngest age group of *ca*. 230 Ma is mainly obtained from the ov3 or pz with minor ov2 domain of Zrn grains which are in contacting with secondary Chl or Ms (Fig. 5). The secondary Ms also replaces secondary And in Crn–Spl-bearing Grt–Crd–Sil granulite (72801B) (Fig. 3c). In addition, the depleted HREE characteristics of these Zrn are distinguishable with other ones (Fig. 6). Therefore, this distinct younger Zrn age group can be interpreted as timing of later hydration resulting in the formation of Chl and Ms at the shallow depth. In case of Crn–Spl-bearing Grt–Crd–Sil granulite (72801B), ov2 domain of Zrn occurring in Crd–

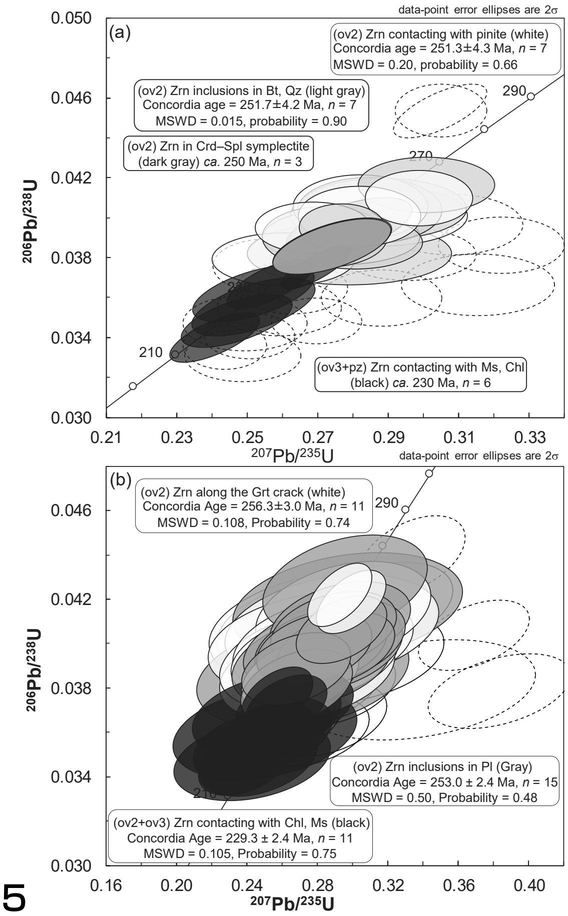

Figure 5

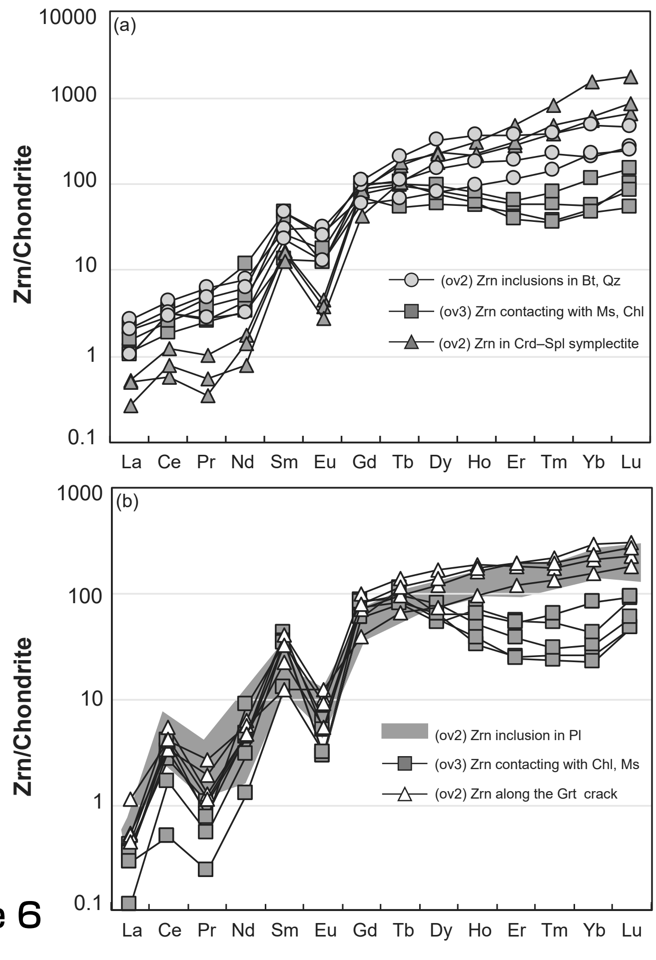

Figure 6

Spl symplectite between Grt and Sil, and Zrn inclusions in Bt and Qz obtained the similar age of *ca*. 250 Ma (Fig. 5a). Nevertheless, the former shows the much more elevated HREE and depleted LREE compared with the later (Fig. 6a). Thus, these two Zrn possibly formed at the same time but by different mechanisms. The Zrn located in Crd–Spl symplectite is considered to be formed by the Grt and Sil breakdown into Spl and Crd through the reaction of Grt+Sil+H_2O→Spl+Crd during decompression stage. The low solubility of Zr as well as not preferring HREE in Crd give the good benefit for Zrn growth (Degeling et al., 2001). The depletion of LREE in these Zrn might be explained by the depleted LREE composition in the reactant Grt. However, due to the morphology, internal texture, REE chemistry and U–Pb age characteristics, the second overgrowth (ov2) of Zrn inclusions in Bt and Qz are expected to be formed from the melt during the HT metamorphism (e.g., Hermann and Rubatto, 2003; Harley et al., 2007). The presence of melt is inferred by the migmatitic occurrence of analyzed samples and subhedral Pl in the matrix (Figs. 2 and 3f). Consequently, the obtained age of *ca*. 250 Ma from these Zrn may indicate for the timing of decompression just after peak metamorphism. In case of Grt–Spl–Crd granulite (72801C), the Zrn inclusions in Pl and Grt (along the crack) yielded slightly older age of *ca*. 250–260 Ma (Fig. 5b). The internal texture and REE chemistry of these Zrn are clearly similar (Figs. 4e, 4g and 6b). Although Zrn in Grt also contacts with secondary Chl filling the Grt crack, the isotopic age and REE feature are distinct from those of Zrn associated with Chl in the matrix (Figs. 5b and 6b). This feature may imply that the Zrn grains included in Grt were not affected by the later hydration event. The internal texture of sector zoning as well as the enrichment of HREE from second overgrowth (ov2) of Zrn inclusions in Pl and Grt the prefer their crystallization from the melt rather than recrystallization by dissolution of their protolith ones (e.g. Harley et al., 2007; Rubatto, 2017). Considering the occurrence of Zrn inside Grt and its slight older age of *ca*. 260 Ma than Zrn in Pl (*ca*. 250 Ma) (Figs. 4g and 5b), the *ca*. 260 Ma age might be interpreted as timing of prograde to peak metamorphism.

In summary, the metamorphic evolution of the high-grade metamorphic rocks in the Kannak Complex, Kontum Massif can be constrained as follows. The pelitic granulites might have undergone the peak UHT condition between *ca*. 260 and 250 Ma by the continental collision in the TVOB (e.g., Osanai et al., 2004). The subsequent decompression stage promoted new Zrn overgrowth by Grt break down or crystallization from the melt at *ca*. 250 Ma, when might correspond to the onset of the exhumation of the Kannak Complex. Finally, the later intense hydration at *ca*. 230 Ma resulted in the abundant formation of secondary Ms and Chl during the exhumation at the shallow depth. Though the duration of the UHT metamorphism in the western Kannak Complex (*ca*. 230–260 Ma) is consistent with that of previous study (e.g., Osanai et al., 2004, 2008; Nakano et al., 2007, 2013), this study provided the critical chronological constraint on the metamorphic history by combining the microscopic observation (mode of occurrences, external and internal texture) and in-situ U–Pb and trace element analyses for Zrn.

Acknowledgments

This study is partly supported by Monbukagakusho/Ministry of Education, Culture, Sports, Science and Technology–Japan (MEXT) scholarship at Kyushu University and JSPS KAKENHI grants Number JP16H02743 and JP22244063 to Y. Osanai and Number JP15K05345 and JP18H01316 to N. Nakano. We appreciated Tran Van Tri, Pham Binh and B.Tamir for their assistance during the field survey in Vietnam. We are also indebted to editor and reviewers for their critical comments regarding the manuscript.

References

Degeling, H., Eggins, S. and Ellis, D.J. (2001) Zr budgets for metamorphic reactions, and the formation of zircon from garnet breakdown. Mineralogical Magazine, 65: 749–758.

Harley, S.L., Kelly, N.M. and Möller, A. (2007) Zircon behaviour and the thermal histories of mountain chains. Elements, 3 (1): 25–30.

Harlry, S.L. (2016) A matter of time: The importance of the duration of UHT metamorphism. Journal of Mineralogy and Petrological Sciences, 111 (2): 50-72.

Hermann, J. and Rubatto D. (2003) Relating zircon and monazite domains to garnet growth zones: age and duration of granulite facies metamorphism in the Val Malenco lower crust. Journal of Metamorphic Geology, 21: 833-852.

Hoskin, P.W.O. and Schaltegger, U. (2003) The composition of zircon and igneous and metamorphic petrogenesis. Reviews in Mineralogy and Geochemistry, 53 (1): 27-62.

Ludwig, K.R. (2008) User's Mnual for Isoplot 3.70: A geochronological toolkit for Microsoft Excel. Berkeley Geochronology Center Special Publication, 4: 1-77.

McDonough, W.F. and Sun, S.S. (1995) Composition of the Earth. Chemical Geology, 120: 223-253.

Nagy, E. A., Maluski, H., Lepvrier, C., Schärer, U., Thi, P.T., Leyreloup, A. and Tich,V.V. (2001) Geodynamic significance of the Kontum massif in central Vietnam: composite $^{40}Ar/^{39}Ar$ and U–Pb ages from Paleozoic to Triassic. The Journal of Geology, 109 (6): 755-770.

Nakano, N., Osanai, Y., Owada, M., Nam, T.N., Toyoshima, T., Binh, P., Tsunogae, T. and Kagami, H. (2007) Geologic and metamorphic evolution of the basement complexes in the Kontum Massif, central Vietnam. Gondwana Research, 12: 438-453.

Nakano, N., Osanai, Y. and Adachi, T. (2010) Major and trace element zoning of euhedral garnet in high-grade (>900 °C) mafic granulite from the Song Ma Suture zone, northern Vietnam. Journal of Mineralogical and Petrological Sciences, 105 (5): 268-273.

Nakano, N., Osanai, Y., Owada, M., Nam, T.N., Charusiri, P. and Khamphavong, K. (2013) Tectonic evolution of high-grade metamorphic terranes in central Vietnam: Constraints from large-scale monazite geochronology. Journal of Asian Earth Sciences, 73 (5): 520-539.

Nam, T.N., Sano, Y., Terada, K., Toriumi, M., Quynh, P.V. and Dung, L.T. (2001) First SHRIMP U–Pb zircon dating of granulites from the Kontum Massif (Vietnam) and tectonothermal implications. Journal of Asian Earth Sciences, 19: 77-84.

Osanai, Y., Nakano, N., Owada, M., Nam, T.N., Toyoshima, T., Tsunogae, T., and Binh, P. (2004) Permo–Triassic ultrahigh-temperature metamorphism in the Kontum Massif, central Vietnam. Journal of Mineralogical and Petrological Sciences, 99 (4): 225-241.

Osanai, Y., Nakano, N., Owada, M., Nam, T.N., Miyamoto, T., Minh, N.T., Nam, N.V. and Tri, T.V. (2008) Collision zone metamorphism in Vietnam and adjacent South-eastern Asia: Proposition for Trans Vietnam Orogenic Belt. Journal of Mineralogical and Petrological Sciences, 103 (4): 226-241.

Owada, M., Osanai, Y., Hokada, T. and Nakano, N. (2006) Timing of metamorphism and formation of garnet granite in the Kontum Massif, central Vietnam: evidence from monazite EMP dating. Journal of Mineralogical and Petrological Sciences, 101 (6): 324-328.

Owada, M., Osanai, Y., Nakano, N., Adachi, T., Kitano, I., Tri, T.V. and Kagami, H. (2016) Late Permian plume-related magmatism and tectonothermal events in the Kontum Massif, central Vietnam. Journal of Mineralogical and Petrological Sciences, 111 (3): 181-195.

Paces, J.B. and Miller, J.D. (1993) Precise U–Pb ages of Duluth Complex and related mafic intrusions, northeastern Minnesota: geochronological insights into physical, petrogenetic, paleomagnetic and tectonomagmatic processes associated with the 1.1 Ga midcontinent rift system. Journal of Geophysical Research, 98: 13997-14013.

Roger, F., Maluski, H., Leyreloup, A., Lepvrier, C. and Thi, P.T. (2007) U–Pb dating of high temperature metamorphic episodes in the Kontum Massif (Vietnam). Journal of Asian Earth Sciences, 30: 565-572.

Rubatto, D. (2017) Zircon: The metamorphic mineral. Reviews in Mineralogy and Geochemistry, 83 (1): 261-295.

Rubatto, D. and Hermann, J. (2007) Experimental zircon/melt and zircon/garnet trace element partitioning and implications for the geochronology of crustal rocks. Chemical Geology, 241: 38-61.

United Nations (1990) Atlas of mineral resources of the ESCAP region, Volume 6, Viet Nam. United Nations Publication, Bangkok, 124.

Whitney, D.L. and Evans, B.W. (2010) Abbreviations for names of rock–forming minerals. American Mineralogist, 95:

185–187.
Wiedenbeck, M., Alle, P., Corfu, F., Griffin, W.L., Meier, M., Oberli, F., von Quadt, A., Roddick, J.C. and Spiegel, W. (1995) Three natural zircon standards for U–Th–Pb, Lu–Hf, trace element and REE analyses. Geostandards Newsletter, 19: 1–23.

Figure caption

Figure 1. Location of the Kontum Massif in Vietnam (a) and distribution of metamorphic rocks as well as intrusive rocks in the Kontum massif (b) after United Nations (1990). Only metamorphic ages for the Kannak Complex reported in previous studies are shown in (b), which is compiled from Navy et al. (2001); Nam et al., (2001); Osanai et al. (2004); Nakano et al. (2007); Roger et al. (2007); Nakano et al. (2013) Locations of analysed samples in this study are also shown as grey circles.

Figure 2. The modes of occurrence for analysed pelitic granulites in the Kannak Complex. (a) Crn–Spl-bearing Grt–Crd–Sil granulite (72801B), (b) Grt–Spl–Crd granulite (72801C). The coarse-grained pinkish Grt with greenish Crd corona and leucocratic pod can be seen by the naked eyes.

Figure 3. Photomicrographs of analyzed samples from the Kannak Complex (a-e) Crn–Spl-bearing Grt–Crd–Sil granulite (72801B). (f-h) Grt–Spl–Crd granulite (72801C). (a) Spl–Crd symplectite surrounding Sil nematoblasts in Crn–Spl-bearing Grt–Crd–Sil granulite. (b) Crn in contact with Bt and Mag. (c) Secondary And is replaced by secondary Ms. (d) Zrn inclusion in Sil nearby Crd–Spl symplectite. (e) Zrn in contact with Ms. (f) Anhedral dark green Spl mainly contact with sub- to euhedral Pl and Mag. Grt crack is filled by Chl and Bt. (g) Zrn inclusions in Grt and secondary Bt. (h) Zrn inclusions in Grt and Pl.

Figure 4. The representative CL images of Zrn with analysis spots, U–Pb age and Th/U ratios for Zrn in Crn–Spl-bearing Grt–Crd–Sil granulite (72801B) (a-d) and Grt–Spl–Crd granulite (72801C) (e-g). 50 μm scale bar is also shown in each figure. The mode of occurrence for each representative analysed Zrn is also present in the right side of each figure. The black circles indicate for the analytical point of U–Pb dating, of which the solid and dash ones for the concordant and discordant data, respectively. The white circles present for the REE analytical location.

Figure 5. Concordia diagrams for the results of LA–ICP–MS Zrn U–Pb dating for Crn–Spl-bearing Grt–Crd–Sil granulite (72801B) (a) and Grt–Spl–Crd granulite (72801C) (b). The concordia age is calculated for each occurrence of Zrn in each sample. In the concordia diagrams, concordant and discordant data are shown with solid and dash ellipses, respectively.

Figure 6. REE pattern normalized by chondrite value for metamorphic Zrn from Crn–Spl-bearing Grt–Crd–Sil granulite (72801B) (a) and Grt–Spl–Crd granulite (72801C) (b). Chondrite values are after McDonough and Sun (1995). See detail in the text.